Plastic deformation behavior of lath martensitic steel focusing on lath boundaries

Ye-eun Na [a], Hadi Ghaffarian [a], Dongchan Jang [a*]
[a]*Department of Nuclear and Quantum Engineering, KAIST, 291 Daehak-ro, Yuseong-gu, Daejeon 34141, Republic of Korea*
[*]*Corresponding author: dongchan.jang@kaist.ac.kr*

1. Introduction

Lath martensitic steel has been developed as structural materials in various industries including nuclear field, due to its high strength and toughness accompanied by thermal stability. It has hierarchical microstructure stem from FCC to BCC phase transformation following Kurdjumov-Sachs (K-S) orientation relationship, i.e. $\{111\}_\gamma \parallel \{110\}_{\alpha'}$ and $< \bar{1}10 >_\gamma \parallel < \bar{1}11 >_{\alpha'}$ [1]. Total 24 variants can be formed from one prior austenite grain and there are 4 different interfaces: packet, block, sub-block and lath boundaries. Several studies about plastic deformation mechanisms about packet and block boundaries have been done [2–4], however the role of low-angle grain boundaries, especially lath boundaries, has not been understood yet.

In this study, we conducted in-situ SEM compression tests on micro-pillars fabricated within a block to figure out the plastic deformation behavior carried out by the lowest microstructural features, lath boundaries.

2. Experimental procedure

The chemical compositions of the investigated sample are given in Table I. It is composed of Cr=9.1, C=0.1, W=1.1, Mn=0.42, V=0.21, Si=0.11, Ta=0.1, Ti=0.015 and the rest with Fe. Normalization was done at 1273 K for 0.5 h and then water-quenched [5]. Two sides of the bulk ingot were mechanically polished down to 0.04 um colloidal silica powders. Then, to remove mechanically-damaged surface layer, electro-polishing was done using 250 ml H_3PO_4+150 ml H_2SO_4+100 ml H_2O.

Based on the image quality (IQ)+inverse pole figure (IPF) map of bulk surface, the positions of micro-pillars were marked using focused ion beam (FIB) with 40 pA. Samples were made in square shaped-pillars and EBSD was taken on both sides to confirm the position of low-angle boundaries within samples. Picoindenter (PI-87, Bruker) was used to perform in-situ SEM micro-compression tests. Compression was performed until we observe clear slip lines via SEM images (total engineering strain was about 5-8%) at a nominal strain rate of 10^{-3}/sec. After compression tests, post-mortem analysis was carried out using SEM, TEM, and in-depth EBSD.

	Cr	C	W	Mn	V	Si	Ta	Ti	Fe
wt%	9.1	0.1	1.1	0.42	0.21	0.11	0.1	0.015	rest

Table I: Chemical compositions of lath martensitic steel in this study.

3. Results and discussion

3.1 Micro-compression tests

Figure 1 shows IQ+IPF maps and BSE images of specimens following two different plastic deformation behavior: (a,b) Grain boundary sliding along lath boundaries, i.e. lath boundary sliding (LBS) and (c,d) lattice slip. Slip traces are clearly matched with lath boundaries in (a) and (b). However, even though there're lath boundaries well-aligned to compression direction, there're cases that didn't carry LBS but followed one of crystallographic slip systems in (c) and (d).

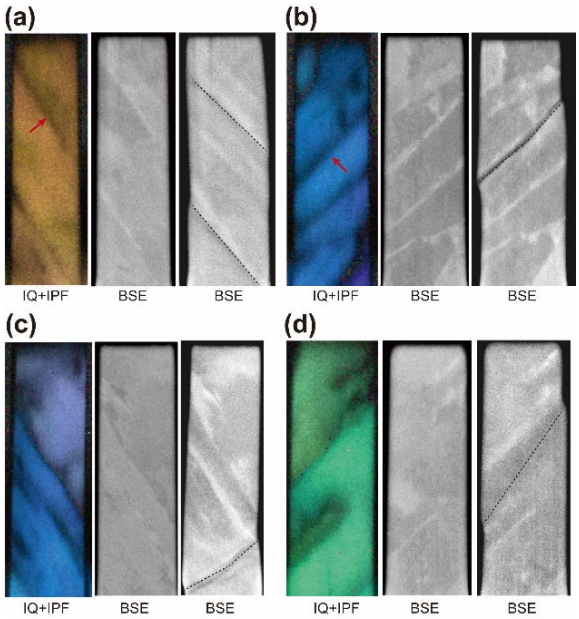

Figure 1. IQ+IPF maps and BSE images of samples with (a,b) lath boundary sliding (LBS) and (c,d) lattice slip, respectively.

3.2 Mechanism of Lath boundary sliding

Previous works about lath boundary sliding insist that there are FCC structured retained austenitic films between laths and it works as a 'greasy' plane and accommodate plastic deformation following the lath boundary plane [6,7]. In our experiment, there was no FCC-structured retained austenitic film but well-organized dislocation networks were found at the lath boundaries as depicted in Figure 2 (a).

Based on the previous studies about crystallography of lath martensite, lath boundary planes, i.e. habit planes, are almost parallel to one of $\{111\}_\gamma \parallel \{110\}_{\alpha'}$ and close to pure twist low-angle grain boundaries. In case of pure twist low-angle boundary on $\{110\}_{BCC}$ plane, there are 3 sets of dislocation arrays called hexagonal dislocation networks (HDNs) inducing sliding by movement of whole network [8]. Also, we observed the HDNs right at the lath boundary where sliding happened as depicted in Figure 2 (b).

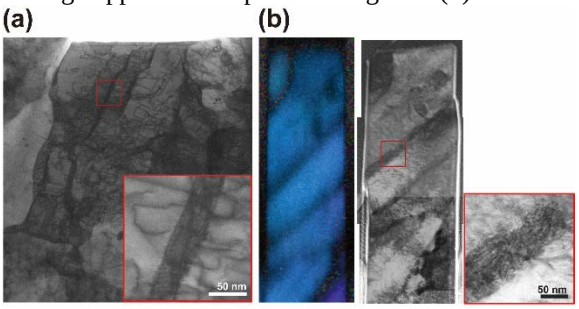

Figure 2. STEM images of hexagonal dislocation networks in lath martensitic steel.

3.3 Conditions for Lath boundary sliding

To figure out the conditions for lath boundary sliding, the misorientation angles and rotation axis $\vec{r}$ were calculated for every lath boundary in this experiments. Figure 3 plots misorientation angle and $|\vec{r} \cdot \vec{n}|$ value and the data within yellow box, where angle is smaller than 4° and $|\vec{r} \cdot \vec{n}|$ value is larger than 0.7, showed lath boundary sliding. However, the ones in grey region didn't show any sliding along lath boundary.

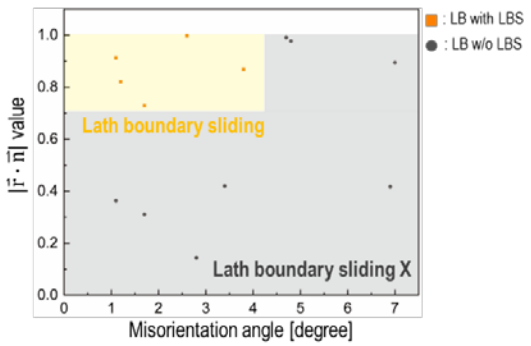

Figure 3. Misorientation angle and $|\vec{r} \cdot \vec{n}|$ value of the lath boundaries. Yellow box indicates the conditions for lath boundary sliding.

3.4 CRSSs of two competing mechanisms

To quantitatively compare the two different plastic deformation mechanism, critical resolved shear stresses (CRSSs) were calculated following equation (1) and (2), where θ is the angle between slip plane normal and force and λ is the angle between slip direction and force (see Figure 4(a)).

$$CRSS_{\text{Lattice slip}} = \sigma_y \cdot \cos\theta \cdot \cos\lambda \quad (1)$$
$$CRSS_{\text{LB sliding}} = \sigma_y \cdot \cos\theta \cdot \sin\theta \quad (2)$$

Following equation (1) and (2), the critical resolved shear stresses of lattice slip and LB sliding are 477 and 404 MPa, respectively. It shows LB sliding has about 15% lower resolved shear stress compared to lattice slip, meaning LB sliding is one of main plastic deformation mechanisms in lath martensitic steel.

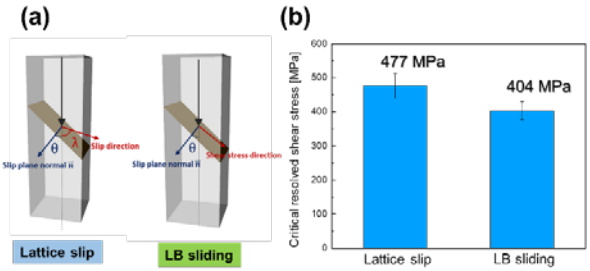

Figure 4. (a) Schematic illustrations about CRSS calculation of lattice slip and LB sliding mechanism. (b) Average CRSS values of lattice slip and LB sliding.

4. Conclusions

In this study, micro-compression tests were performed with rigorous EBSD and TEM analysis. We reached the following conclusions:

- Hexagonal dislocation networks (HDNs) are formed on lath boundary plane close to pure twist low-angle grain boundary and their movement mediate lath boundary sliding.
- To facilitate lath boundary sliding (LBS) mechanism, misorientation angle should be smaller than 4° and $|\vec{r} \cdot \vec{n}|$ value higher than 0.7, i.e. the boundary should be close to pure twist low-angle grain boundary.
- Critical resolved shear stresses (CRSSs) of LBS and lattice slip are 404 and 477 MPa, respectively. LBS shows about 15% lower CRSS than lattice slip.
- Lath boundary sliding is one of important plastic deformation mechanisms in lath martensitic steel.

References

[1] S. Morito, H. Tanaka, R. Konishi, T. Furuhara, T. Maki, The morphology and crystallography of lath martensite in Fe-C alloys, Acta Mater. 51 (2003) 1789–1799. https://doi.org/10.1016/S1359-6454(02)00577-3.

[2] Y. Mine, K. Hirashita, H. Takashima, M. Matsuda, K. Takashima, Micro-tension behaviour of lath martensite structures of carbon steel, Mater. Sci. Eng. A. 560 (2013) 535–544. https://doi.org/10.1016/j.msea.2012.09.099.

[3] A. Shibata, T. Nagoshi, M. Sone, S. Morito, Y. Higo, Evaluation of the block boundary and sub-block boundary strengths of ferrous lath martensite using a micro-bending test, Mater. Sci. Eng. A. 527 (2010) 7538–7544. https://doi.org/10.1016/j.msea.2010.08.026.

[4] C. Du, J.P.M. Hoefnagels, R. Vaes, M.G.D. Geers, Block and sub-block boundary strengthening in lath martensite, Scr. Mater. 116 (2016) 117–121. https://doi.org/10.1016/j.scriptamat.2016.01.043.

[5] H.K. Kim, J.W. Lee, J. Moon, C.H. Lee, H.U. Hong, Effects of Ti and Ta addition on microstructure stability and tensile properties of reduced activation ferritic/martensitic steel for nuclear fusion reactors, J. Nucl. Mater. 500 (2018) 327–336. https://doi.org/10.1016/j.jnucmat.2018.01.008.

[6] C. Du, J.P.M. Hoefnagels, R. Vaes, M.G.D. Geers, Plasticity of lath martensite by sliding of substructure boundaries, Scr. Mater. 120 (2016) 37–40. https://doi.org/10.1016/j.scriptamat.2016.04.006.

[7] F. Maresca, V.G. Kouznetsova, M.G.D. Geers, On the role of interlath retained austenite in the deformation of lath martensite, Model. Simul. Mater. Sci. Eng. 22 (2014). https://doi.org/10.1088/0965-0393/22/4/045011.

[8] Z.Y. Xia, Z.J. Zhang, J.X. Yan, J.B. Yang, Z.F. Zhang, General yield behaviors of the {1 1 0} hexagonal dislocation networks in body centered cubic metal molybdenum, Comput. Mater. Sci. 170 (2019) 109116. https://doi.org/10.1016/j.commatsci.2019.109116.